Atmos. Chem. Phys. Discuss., 14, 21565–21609, 2014
www.atmos-chem-phys-discuss.net/14/21565/2014/
doi:10.5194/acpd-14-21565-2014

Atmospheric Chemistry and Physics Discussions

Aqueous phase oligomerization of methyl vinyl ketone through photooxidation – Part 2: Development of the chemical mechanism and atmospheric implications

B. Ervens[1,2], P. Renard[3], S. Ravier[3], J.-L. Clément[4], and A. Monod[3]

[1]Cooperative Institute for Research in Environmental Sciences, University of Colorado, Boulder, Colorado, USA
[2]Chemical Sciences Division, NOAA Earth System Research Laboratory, Boulder, Colorado, USA
[3]Aix Marseille Université CNRS, LCE FRE 3416, 13331, Marseille, France
[4]Aix Marseille Université CNRS, ICR UMR7273, 13397, Marseille, France

Received: 29 July 2014 – Accepted: 3 August 2014 – Published: 22 August 2014

Correspondence to: B. Ervens (barbara.ervens@noaa.gov)

Published by Copernicus Publications on behalf of the European Geosciences Union.

Abstract

We developed a chemical mechanism based on laboratory experiments that have shown efficient oligomerization from methyl vinyl ketone (MVK) in the bulk aqueous phase. Kinetic data are applied (if known) or fitted to the observed MVK decay and oligomer mass increase. The mechanism is then implemented into a multiphase box model that simulates (i) oligomer formation upon uptake of MVK from the gas phase, and (ii) SOA formation from isoprene, as a precursor of MVK and methacrolein (MACR) in the aqueous and gas phases.

Model results show that under atmospheric conditions, the oligomer formation rate strongly depends on the availability of dissolved oxygen. If oxygen is consumed too quickly or its solubility is kinetically or thermodynamically limited, oligomerization is accelerated, in agreement with the laboratory studies. The comparison of predicted oligomer formation shows that for most model assumptions (e.g. depending on the assumed partitioning of MVK and MACR), SOA formation from isoprene in the gas phase exceeds aqueous SOA formation by a factor 3–4. However, at high aerosol liquid water content and potentially high partitioning of oligomer precursors into the aqueous phase, SOA formation in both phases might be equally efficient.

1 Introduction

Organic aerosol particles in the atmosphere comprise about 50 % of the total particulate matter mass (Zhang et al., 2007). A small fraction of them are emitted directly by various sources (primary organic aerosol, POA); the major portion is formed by chemical and/or physical processes during their residence time in the atmosphere (secondary organic aerosol, SOA) (Kanakidou et al., 2005). Traditionally, it has been assumed that SOA is formed by condensation of low-volatility or semivolatile organic products that represent gas phase oxidation products from emitted precursor compounds. SOA formation from such products ("gasSOA") is often described by the

ACPD
14, 21565–21609, 2014

two-product model (Odum et al., 1996) or, more recently, by the volatility basis set (VBS) (e.g., Donahue et al., 2006, 2011; Trump and Donahue, 2014). While this mechanism can explain a large amount of observed ambient SOA mass, specific SOA properties (e.g. high oxygen-to-carbon (O/C) ratio) and individual compounds, e.g., dicarboxylic acids, oligomers, cannot be predicted by chemical reactions in the gas phase.

Several recent laboratory, field and model studies point to efficient chemical reactions in the aqueous phase of cloud/fog droplets and aerosol particles that lead to low volatility products that remain in the particle phase upon water evaporation ("aqSOA", Ervens et al., 2011). However, the contribution of secondary organic aerosol formation in the aqueous phase of aerosol particles and in cloud or fog droplets to total ambient SOA loading has not been quantified yet due to the poor mechanistic understanding, which makes a comprehensive implementation in models difficult and ambiguous. Systematic laboratory experiments have been performed in order to elucidate the SOA formation potential of various precursors such as small carbonyl compounds (Kalberer et al., 2004; Tolocka et al., 2004; Lim et al., 2010; Ervens et al., 2011 and references therein). Several laboratory experiments focused on SOA precursors that are formed from isoprene. Isoprene emission rates exceed those of all other anthropogenic and biogenic organics, and, thus even a small yield (< 5 %) might significantly contribute to the total SOA burden (Carlton et al., 2009). Isoprene is not very water-soluble ($K_{H,isoprene} = 0.013\,M\,atm^{-1}$, Mackay and Shiu, 1981) and, thus, its fraction in the atmospheric aqueous phases is < 0.001 %, related to the total atmospheric isoprene concentration. Its first-generation oxidation products, methyl vinyl ketone (MVK) and methacrolein (MACR), are more soluble ($K_{H,MACR} = 6.5\,M\,atm^{-1}$; $K_{H,MVK} = 41\,M\,atm^{-1}$, Iraci et al., 1999), but, yet, their aqueous phase fractions in pure water is < 1 %. However, simultaneous measurements of similar small carbonyl compounds in the gas and particle phases have shown that a substantial fraction of them might be associated with the particulate phase (Baboukas et al., 2000; Matsunaga et al., 2005; Kawamura et al., 2013) and thus accumulate in aerosol water.

ACPD
14, 21565–21609, 2014

Several recent laboratory studies have explored the reactivity of MVK and MACR in the aqueous phase, and depending on the initial concentration, efficient formation of oligomeric compounds has been observed (Zhang et al., 2010; Renard et al., 2013). Organic compounds with oligomeric (or polymeric) structures have also been identified in ambient aerosol particles (Denkenberger et al., 2007; Polidori et al., 2008; Mazzoleni et al., 2010; Zhang and Ying, 2011) as well as in rainwater (Altieri et al., 2009; Mead et al., 2013). However, to date the explicit chemical pathways leading to oligomers are not fully implemented into atmospheric chemistry models since the chemical mechanisms are not available. The current study aims at (partially) closing this gap by presenting the kinetic and mechanistic details of chemical pathways to explain the observed oligomer formation from MVK during the bulk aqueous phase experiments that were presented by Renard et al. (2013), and in the companion paper of this study (Renard et al., 2014, referred to as "Part I" hereafter). By fitting kinetic rate constants and combining them with known constants for basic chemical processes, a comprehensive chemical mechanism for the oligomerization of MVK in the aqueous phase is derived (Sect. 2). This mechanism is used in a multiphase box model and sensitivities of the oligomerization rate to various microphysical (liquid water content, surface–volume ratio) and physicochemical (solubility of MVK and oxygen) parameters are explored (Sect. 3). Finally, the question is explored under what atmospheric conditions aqSOA formation from isoprene might be similarly important as gasSOA formation from its precursor. For this estimate, we include similar reaction patterns in the aqueous phase for MACR as for MVK (Sect. 4).

ACPD
14, 21565–21609, 2014

2 Experiment-model comparisons

2.1 Chemical mechanism development

2.1.1 Kinetic data for individual processes

The analysis of the resulting oligomers was performed by ultra-high-performance liquid chromatography mass spectrometry (UPLC-ESI-MS). All analytical methods are discussed in detail in Part I. In brief, the temporal evolution of the MVK and O_2 aqueous concentrations were recorded during the laboratory experiments using liquid chromatography UV absorbance spectroscopy (UPLC-UV, for MVK and H_2O_2 concentrations). Dissolved oxygen concentration and pH were recorded by a multi-parameter analyzer (Consort C3020). The OH concentration in the aqueous phase could not be directly measured. However, it could be derived based on the observed photolytic loss of hydrogen peroxide. Experiments in the absence of MVK revealed a photolysis rate of $1.01 \times 10^{-5}\,s^{-1}$. This rate decreased with as a function of MVK concentrations (Sect. 2.2.2). Cross reactions of OH, HO_x and H_2O_2 were included to account for the recycling of these species (HO_x reactions in Table 1). The chemical mechanism of MVK decay and oligomer formation as suggested by Renard et al. (2013) has been adapted here with some minor modifications in order to constrain the kinetic data (Fig. 1). Not all intermediates were detected during the experiments; however, the structure of the resulting oligomers was used to deduce the suggested reaction pathways. As an α, β-unsaturated carbonyl, MVK bears highly reactive functional groups, i.e., conjugated carbon-carbon and carbon-oxygen double bonds. Therefore, its oxidation by OH might occur via three reaction channels: OH might add to the vinyl group of the MVK molecule either on (1) the β-carbon atom or on (2) the α-carbon atom, or (3) it might abstract a hydrogen atom from either the vinyl group or the saturated end of the molecule. Pathways (1) and (2) lead to isomeric hydroxyalkyl radicals with identical molecular weights and, thus, neither the initiator radicals nor the resulting oligomers, respectively, are distinguishable with the analytical techniques (mass spectrometry) applied

ACPD
14, 21565–21609, 2014

here. Theoretically, OH addition on the β-carbon atom (pathway 1) is favored on both steric and resonance grounds; the propagating radical formed by this pathway (1) is the more stable one (Odian, 2004). An attempt to distinguish between the three pathways was performed by direct observation of the resulting alkyl radicals using continuous-flow electron paramagnetic resonance (EPR) experiments with MVK concentrations from 1 to 25 mM (Sect. S1 in the Supplement). The obtained highly complex spectra were the result of superimposition of various EPR signals. Using spectral simulations, the signal of HO-CH_2–CH–C(O)CH_3 radical adduct resulting from pathway (1) was clearly distinguished (dots in Fig. S1). The proportions of another transient radical was found to depend on the initial MVK concentration (compare the spectra in Figs. S1.1 and S1.2 in the Supplement). A very similar behavior of concentration-dependency of radical species was previously observed in experiments performed on acrylic acid by Gilbert et al. (1994), and they attributed this behavior to the formation of dimer radicals. Therefore, our concentration-dependent radical was attributed to a dimer radical such as HO-CH_2-CH(C(O)CH_3)-CH_2-CH-C(O)CH_3, thus confirming the very fast oligomerization (recombination) pathway (Gilbert et al., 1994). More than two different radical species were present in our experiments, but their respective signals remained unidentified due to overlapping EPR signals in the spectra. Although it was not possible to identify these other radical species, the occurrence of radicals resulting from pathways (2) and (3) was expected, and the EPR experiments showed that their relative importance was much lower than that of pathway (1). In the model, we lump pathways (1) and (2) to the more likely radical from pathway (1) ($k_{\mathrm{MVKOH(a)}}$, Fig. 1). H-abstraction (pathway 3) might occur most likely on the most weakly bonded H atoms, which are the ones in the methyl group (bond energy $\sim 94\,\mathrm{kcal\,mol^{-1}}$, as opposed to $\sim 111\,\mathrm{kcal\,mol^{-1}}$ for the other H-atoms of the molecule, Blanksby and Ellison, 2003) and stabilization of the resulting radical due to the adjacent carbonyl group. The rate constant for the reaction of MVK with OH has been recently determined as $k_{\mathrm{MVKOH}} = 7.3 \times 10^{9}\,\mathrm{M^{-1}\,s^{-1}}$ (Schöne et al., 2014). Due to the lack of the exact rate constants for the different branching reactions, we assume that pathway (3) might occur with a similar rate constant as

ACPD
14, 21565–21609, 2014

H-abstraction from the structurally-similar acetone ($k_{OH,Acetone} = 1.2 \times 10^8\,M^{-1}\,s^{-1}$, Ervens et al., 2003; Monod et al., 2005). The ratio $k_{OH,Acetone}/k_{MVKOH} \sim 1.6\,\%$ is in qualitatively good agreement with the EPR results that suggest a minor contribution of the H-abstraction pathway. The resulting alkyl radicals can react with dissolved oxygen to form peroxy radicals RO_2. The rate constant for this step for all radicals is assumed to be nearly diffusion controlled with $k_{O_2} = 3.1 \times 10^9\,M^{-1}\,s^{-1}$ based on the overview by Neta et al. (1990). In previous model efforts to fit experiments of small organic compounds in aqueous solution, it was assumed that k_{O_2} could be substantially smaller ($k_{O_2} \sim 10^6\,M^{-1}\,s^{-1}$) (Guzman et al., 2006; Lim et al., 2010, 2013). However, a literature review of rate constants for numerous similar compounds (Alfassi, 1997) reveals that all constants for such reactions are in a range of $2 \times 10^9\,M^{-1}\,s^{-1} < k_{O_2} < 4 \times 10^9\,M^{-1}\,s^{-1}$. Only for non-carbon-centered radicals (such as nitrogen-centered radicals), significantly smaller rate constants are observed ($\sim 10^7$–$10^8\,M^{-1}\,s^{-1}$), and none of them is as low as $k_{O_2} \sim 10^6\,M^{-1}\,s^{-1}$. An explanation for this discrepancy is the continuous depletion of oxygen during the reactant consumption (Sect. 2.2.3) that leads to a decrease of the reaction rate (i.e., the product of rate constant and concentration) with time. Thus, we suggest that in the previous experiments, the solutions were temporarily depleted in dissolved oxygen but occurred with rate constants similar to k_{O_2} as used in the current study. In addition to the reaction with oxygen, the alkyl radicals can react with MVK (k_{olig}) by opening its double bond and forming larger molecules (oligomer radicals). This process leads to large radicals that contain multiple MVK units and can recombine to form non-radical oligomers (Sect. 2.1.2).

At various places in the mechanism, rearrangement and recombination reactions of radicals are inferred (k_{arr} and k_{recomb}, respectively). Their rate constants do not have a large influence on the overall oligomer formation rate that is largely determined by k_{olig} and k_{loss}. Since data for the exact compounds are not available, they have been estimated based on those for structurally- similar compounds (NDRL/NIST, 2002). These steps are assumed based on the carbon structure of the resulting detected oligomers. Due to the lack of detailed data on the photolysis of organic hydroperoxides,

ACPD
14, 21565–21609, 2014

all photolysis processes of such compounds were assumed to occur with the same rate as H_2O_2 photolysis (Sect. 2.2.2). This assumption is supported by the similar aqueous phase photolysis rate constants of CH_3OOH, C_2H_5OOH and H_2O_2 (Monod et al., 2000, 2007).

2.1.2 Model treatment of oligomer series

The evolution of the oligomer mass exhibits a three-step kinetics that is characterized by different slopes, i.e., an initial slow increase, when oligomerization is not very efficient yet, a fast increase and a later decrease (cf Figs. 3 and 6 in Part I). The observed oligomer increase and decrease, together with the determined mass yield were used to constrain the rate constants in the chemical mechanism for oligomer formation and loss (k_{olig}, k_{loss} in Fig. 1, respectively). Renard et al. (2013) identified thirteen oligomer series, among which seven series differed in their initiator radical. Each oligomer series showed the typical "haystack" pattern in the mass spectrum where signals differed by $\Delta m/z$ 70.0419 (exactly corresponding to the molecular mass of MVK). The addition of similar unsaturated compounds to initiator radicals usually occurs with rate constants in the range of $10^2\,M^{-1}\,s^{-1} < k_{olig} < 10^4\,M^{-1}\,s^{-1}$ (Odian, 2004). However, even applying the upper limit of this range did not lead to sufficiently fast MVK decay and oligomer increase as compared to the observed behavior. Only a value of $k_{olig} = 5 \times 10^7\,M^{-1}\,s^{-1}$ gave a reasonable match between observed and modeled data. The reasons for this discrepancy to literature values are not clear; they might include the facts that (i) no specific kinetic data for MVK oligomerization are available, and this compound may have a higher reactivity than other species and/or (ii) not all MVK-consuming processes are included in the mechanism in Fig. 1. Such potentially missing pathways will also lead to oligomers, since the predicted oligomer total mass yield from the developed chemical mechanism is similar to the observed one. For all series, we consider the formation of oligomers with up to ten MVK molecules, in agreement with the experimental data that showed most oligomer series had a degree of polymerization (n) ≤ 10 (with an average n = 5).

ACPD
14, 21565–21609, 2014

In the termination step of the radical reaction chain (k^{1st}), the oligomer radicals recombine and disproportionate to form one saturated and one unsaturated product, i.e., yielding compound pairs with $\Delta m/z = 2.0157$. In our chemical mechanism, these oligomer pairs are lumped into one species per series (Oligomers I, III–VII, Fig. 1). Only Oligomer II is explicitly represented, since it is the only one that originates from peroxy radicals. It does not form by recombination reaction with itself, but by reaction with the more abundant HO_2 radical. The intermediate radicals are treated explicitly in the mechanism, i.e., 70 different radicals from seven initiator radicals for series I–VII with up to n MVK molecules ($1 \leq n \leq 10$), whereas the resulting oligomers are lumped into one single compound per series. For simplicity, we parameterized the termination step by a process of first-order kinetics (k^{1st}). In the literature, second-order rate constants of termination reactions in radical oligomerization are typically in the range of 10^7–$10^9\,M^{-1}\,s^{-1}$ (Long et al., 2001). Since these are second-order rate constants, this range is not directly comparable to the fitted value of $k^{1st} = 6 \times 10^4\,s^{-1}$, but implies that the total radical concentrations might be on the order of $\sim 10^{-5}$–10^{-3} M, which seems reasonable in the relatively highly concentrated solutions used here. Our mechanism is somewhat simplified, since it is assumed that recombination reactions only occur between molecules of the same series. In reality, these recombination reactions can occur between all radicals. However, since the number of processes in our model would become untraceable for recombination between all 70 radicals ($\sim$ 5000 possible processes), we chose to only include recombination reactions within the same series. If all possible recombination reactions were taken into account, k^{1st} might be smaller since the same reaction rate could be predicted by assuming a higher radical concentration.

The experiments showed that the oligomers continue to react and decrease (Figs. 7–9 in Part I). It is assumed that this loss is caused by the continuous oxidation of oligomers by OH or by direct photolysis. For simplicity, we describe this loss in the model exclusively by the OH radical, even though direct photolysis of carbonyl compounds might be at least as efficient as OH reaction as a loss process (Epstein et al., 2013; Reed-Harris et al., 2014). The fitted OH rate constant ($k_{loss} = 10^8\,M^{-1}\,s^{-1}$) is

ACPD
14, 21565–21609, 2014

on the same order of magnitude as for other large carbonyl compounds (Doussin and Monod, 2013).

2.2 Experiment-model comparison: 0.2 mM ≤ $[MVK]_0$ ≤ 20 mM

2.2.1 Input data to the box model

Five laboratory experiments were carried out that differed in the initial MVK concentration ($[MVK]_0$ = 0.2 mM, 2 mM, 5 mM, and 20 mM, respectively). The ratio of initial MVK and H_2O_2 was constant in all experiments ($[MVK]_0/[H_2O_2]_0$ = 0.05), in order to favor the reaction of OH with MVK over its reaction with H_2O_2 by more than 90 %. The initial concentration of dissolved oxygen was different for the various initial H_2O_2 concentrations ($[O_2]_0$ = 284 µM, 358 µM, 436 µM and 505 µM for the four initial MVK concentrations). An additional experiment with $[MVK]_0$ = 20 mM was also performed in a nearly deoxygenated bulk aqueous phase where $[O_2]_0 \sim 60$ µM. The concentration of dissolved oxygen was highly variable with time and was continuously measured over the course of the experiments. The solutions were continuously stirred during the experiments. In order to constrain the oxygen concentration in the model, the measured oxygen concentrations for all experiments were fitted and the derived numerical approximations (Sect. S2 in the Supplement) were used as input data to the box model since mixing (stirring) effects between gas and aqueous phases cannot be reproduced within our simple model framework. The observed increase in dissolved oxygen towards the end of the experiments (Fig. S2a–e) can be explained by oxygen formation in the recombination reactions of HO_2/O_2^- with HO_2 and OH radicals, once MVK is nearly consumed (Table 1). While this reaction always occurs over the course of the experiments, towards the end of the experiments, insufficient organic compounds are available to form alkyl radicals that could efficiently consume oxygen.

A decrease in pH was observed from pH ∼ 6 to ∼ 3 for experiments with $[MVK]_0 \geq$ 2 mM and to pH ∼ 4 for $[MVK]_0 \geq$ 0.2 mM. This evolution was approximated by linear fits as input to the box model (Sect. S3 in the Supplement). This decrease in pH is likely

ACPD
14, 21565–21609, 2014

caused by the formation of organic acids, such as acetic and pyruvic acids (Fig. 1) and possibly other compounds with acid functionalities that are formed upon oligomer decay (k_{loss}) as shown in Part I. These products are not further tracked in the mechanism.

2.2.2 H_2O_2 photolysis rates as a function of $[MVK]_0$

The initial decay of MVK is only determined by its reactions with the OH radical ($k_{MVKOH(a)}$ and $k_{MVKOH(b)}$, Fig. 1 and Table 1). Once a sufficiently high concentration of organic alkyl radicals is present, when most of the dissolved O_2 is consumed, efficient oligomerization starts, which leads to additional loss of MVK. This transition from MVK consumption by only OH to that due to oligomerization can be seen by the two different slopes, denoted by the small blue arrows in Fig. 2a and b, where it is most pronounced as compared to less clear features at lower $[MVK]_0$. Since the initial MVK concentration and k_{MVKOH} are known, the only unknown value in determining the initial MVK loss rate is the OH radical concentration in the aqueous phase, which cannot be directly measured. In independent experiments, in the absence of MVK, the loss of H_2O_2 in the aqueous phase was measured ($j_{H_2O_2}$). The photolysis rate should be independent of the initial H_2O_2 concentration and was determined as $j_{H_2O_2} = 1.01 \times 10^{-5}\,s^{-1}$. However, using this value to simulate the initial decay of MVK led to a significant overestimate of this reaction rate, i.e., to a too efficient consumption of MVK, with the largest bias for experiments with the highest $[MVK]_0$. This finding suggests that the amount of MVK in the solution affects the H_2O_2 photolysis rate. Control experiments showed that, although MVK absorbs light above 300 nm (Renard et al., 2013), loss by direct photolysis is negligible compared to oxidation by OH. As $j_{H_2O_2}$ is proportional to the incident light intensity, it is likely that its values were sensitive to the amount of absorbed light by MVK, depending on its concentration. Upon this finding, the intensity of the 1000 Watt Xenon arc lamp (LSH 601, Oriel) at eight different wavelengths (327 nm $\leq \lambda \leq$ 337 nm) was determined as a function of MVK aqueous concentrations by means of a spectrophotometer (SR-501, LOT-Oriel) placed under the photoreactor's pyrex double wall (Fig. 3). The decay in light intensity can be explained

ACPD
14, 21565–21609, 2014

by absorption of light due to the conjugated double bonds in MVK that cause strong absorption at 211 nm and weak absorption at 296 nm (Renard et al., 2013). At the highest MVK concentration ($[MVK]_0$ = 20 mM), the light intensity is approximately an order of magnitude lower than in the absence of MVK. Superimposed to these data are the resulting $j_{H_2O_2}$ values that were fitted to match the initial MVK decay (Fig. 3) as a function of the MVK concentration. These values differ by a factor of ∼ 40 between the value for the lowest and highest initial MVK concentrations, respectively. The different data in Fig. 3 show that the relationship between reduction in light intensity and resulting H_2O_2 photolysis rate are in reasonable agreement.

2.2.3 Predicted MVK decay

Comparison of the MVK decay to the evolution of dissolved oxygen (Figs. 2 and S2) shows that MVK consumption accelerates when oxygen is (mostly) consumed. Under such conditions, the reactions of organic radicals with oxygen (k_{O_2} in Fig. 1) become negligible, and oligomerization under nearly anaerobic conditions takes place. At low $[MVK]_0$ (0.2 mM), the MVK consumption occurs over much shorter time scales than at higher initial concentrations, and the competition between OH reaction and oligomerization is not clearly seen. Figure 2e shows MVK decay for $[MVK]_0$ = 20 mM under initially low O_2 conditions, for which the reaction solution was saturated with argon. In comparison to Fig. 2a, it is obvious that the initial slow MVK decay is missing, and MVK is quickly consumed as of the beginning of the experiment. Note the different time scales in the figures that clearly show that the reaction is completed within about half of the time at low oxygen concentrations. This sensitivity to oxygen concentrations is in agreement with the general faster oligomerization rate under low oxygen conditions that is well known from polymer chemistry (Odian, 2004; Mendez et al., 2013). While the reaction cell represents an aqueous volume with a very small surface/volume ratio, the extent will be explored in Sect. 3.2.2 to which such oxygen depletion might occur in atmospheric multiphase systems due to limited oxygen uptake from the gas phase.

ACPD
14, 21565–21609, 2014

2.2.4 Predicted oligomer formation and decay

Figure 4 shows a qualitative comparison of predicted and observed temporal evolution of the total oligomers for the five cases depicted in Fig. 2. The observed total oligomer mass and yield were determined by means of scanning mobility particle sizer (SMPS) measurements of the nebulized solutions (cf. Part I). The oligomer mass represents a net yield, since it is the steady-state concentration from simultaneous oligomer formation (k^{1st}) and loss (k_{loss}) (Fig. 1). Despite different units, we compare the temporal evolution and the relative differences for the predicted oligomer concentrations for the four initial concentrations (and low oxygen for $[MVK]_0 = 20$ mM) (Fig. 4a). Assuming an average molecular weight for all oligomers (mass for initiator radical $+n \cdot$ MVK units ($n = 5$)) the two units can be linearly converted; however, for model purposes, we show all model results in M. The predicted differences of oligomer concentrations between $[MVK]_0 = 20$ mM and $[MVK]_0 = 2$ mM are 1–2 orders of magnitude, in agreement with the experiments. At even lower $[MVK]_0 = 0.2$ mM, oligomer formation becomes very inefficient. Reasons of this discrepancy might include the formation of small, volatile compounds, such as (di)acids, that are not explicitly treated by the model. Both experimental and model data show that at the highest $[MVK]_0$, oligomer mass keeps increasing beyond the experimental time scale ($t = 5000$ s), whereas it is decaying for the lower $[MVK]_0$. This behavior is in agreement with the results shown in Fig. 2, where it is shown that for the lower initial concentrations, MVK is essentially consumed at that time, and no further oligomers can be formed and the loss reaction dominates. While it has been discussed in Part I that oligomer formation is characterized by an initially slow increase in mass, followed by a fast increase and then a decrease, the first step is somewhat obscured in Fig. 4 due to the logarithmic scale. Model results for $[MVK]_0 = 20$ mM for high and low dissolved oxygen, respectively, shows initially a much higher oligomerization rate for the latter case, in agreement with the more efficient and faster MVK decay in Fig. 2e as compared to Fig. 2a. Comparison of the oligomer

ACPD
14, 21565–21609, 2014

increase to experimental data for the "low oxygen case" is not performed, since it was not recorded during the experiments.

The predicted evolution of individual oligomer series is shown in Fig. 5 for $[MVK]_0$ = 20 mM under conditions of high and low initial oxygen concentration. At high initial oxygen concentration, Oligomer II (Fig. 1) is the main contributor to the total oligomer concentration. This oligomer series is the only one that is directly formed from a peroxy radical whereas all others are formed from alkyl radicals and thus are suppressed as long as dissolved oxygen is available. As expected, under low oxygen conditions, the concentration of Oligomer II is (much) smaller and Oligomer I has the highest concentration. Despite the lower oxygen concentration, the resulting concentration of Oligomer II is decreased by about an order of magnitude, but it still has the second highest concentration, followed by Oligomers III and VII. These oligomers need the fewest reaction steps with (assumed) unity yield and, thus, form most efficiently as opposed to those at the bottom of Fig. 1 (Oligomers IV, V, and VI).

UPLC-ESI mass spectra of the product distribution upon MVK oxidation and oligomerization showed that the concentration maximum of the individual series occurred at ~ 5400 s of photooxidation. At that reaction time, assuming the oligomer relative concentrations were proportional to the relative mass spectra peak intensities, the concentrations of all detected oligomer series were in a range of two orders of magnitude (Renard et al., 2013); in the mass spectra data treatment, any series that contributed < 1 % as the most intense peak was ignored. This result is not quite in agreement with the model results shown in Fig. 5, where the spread between the different oligomer concentrations spans about four orders of magnitude. This discrepancy might be due to our simplified assumptions that all oligomerization steps occur with the same rate constant, independently of their initiator radical and of their chain length. Odian (2004) showed that (i) oligomerization slows down with increasing degree of polymerization (n) and (ii) the initial oligomerization rates for small n might be different for different initiator radicals. Due to the lack of any detailed information on these explicit steps and trends for the individual oligomer series in our mechanism, we did not

ACPD
14, 21565–21609, 2014

perform any further refinement of the rate constants. Instead in the following section, we limit our discussion to the prediction of total oligomers, i.e., the sum of Oligomers I–VII since the total mass yield (nearly 100 %) is in agreement with experiments.

3 Multiphase simulations

3.1 Description of the box model and initial conditions

In order to assess the importance of MVK oligomerization as an aqSOA source under atmospheric conditions, we apply the same box model as in Sect. 2. However, instead of initializing MVK, H_2O_2 and O_2 in the aqueous phase, gas phase species are initialized, and their uptake into the aqueous phase of aerosol particles is described by the resistance model (Schwartz, 1986). Initial gas phase mixing ratios and uptake parameters are summarized in Table 2. In the atmospheric multiphase system, MVK is also oxidized in the gas phase by OH; other sinks that are likely less important (direct photolysis, reaction with O_3) are not considered here. It is assumed that both H_2O_2 and O_2 have constant gas phase mixing ratios over the course of the simulations (1 ppb and 0.21 atm, respectively).

The aqueous phase is composed of aqueous particles with a diameter of D_{wet} = 200 nm and a concentration $N_a = 5000\,cm^{-3}$, which gives a total liquid water content of LWC $\sim 20\,\mu g\,m^{-3}$, being typical for deliquesced aerosol particle loadings in the atmosphere. In order to mimic the enhanced partitioning of carbonyl compounds into aerosol water as compared to pure water (Kroll et al., 2005; Matsunaga et al., 2005; Healy et al., 2008; Volkamer et al., 2009; Kawamura et al., 2013), we assume an effective Henry's law constant $K^*_{H,MVK} = 2.1 \times 10^6\,M\,atm^{-1}$. This constant is about 50 000 times higher than that determined in pure water $K_{H,MVK} = 41\,M\,atm^{-1}$ (Iraci et al., 1999), and about three orders of magnitude higher than that determined for MVK in concentrated sulfuric acid solutions (80 %) ($K_{H,MVK} = 3000\,M\,atm^{-1}$, Noziere et al., 2006). To date, it is not fully clear which parameters or processes lead to this enhanced partitioning;

ACPD
14, 21565–21609, 2014

interactions with the carbonyl compounds with inorganic ions in the aqueous phase might contribute to it (Yu et al., 2011). Another factor might be the accumulation of MVK and its oligomers near the air/water interface as observed for other compounds (Donaldson and Valsaraj, 2010). Such separation from the bulk aqueous phase would favor heterogeneous reactions occurring at the interface, where organic concentrations are enhanced as compared to the bulk. While such systems cannot be accurately described by Henry's law constants, the assumption of a higher K_H to account for enhanced partitioning to the condensed phase might be considered as a proxy to represent such a behavior. There are no observations specifically for MVK available for proxy or ambient aerosol water. However, our assumption of $K^*_{H,MVK}$ implies that it behaves similarly to aliphatic carbonyl compounds such as glyoxal, methylglyoxal, hydroxyacetone. This $K^*_{H,MVK}$ value results in a MVK fraction in the aqueous phase of 0.1 %, and an aqueous phase concentration of ∼ 2 mM, that can be considered as being typical for organics in aerosol water (Lim et al., 2010) and is within the range of the concentrations that were used in the laboratory experiments.

3.2 Model sensitivity studies

The sensitivity to oligomer formation is explored by multiple simulations where one parameter at a time in Table 2 is varied. The various model cases are listed in Table 3. A recent study has highlighted that the aerosol surface, or more specifically, the surface-volume ratio of aqueous aerosol particles might limit the amount of OH-initiated aqSOA mass (Ervens et al., 2014), since the limited uptake of OH might control organic oxidation reactions in the aqueous phase. Case B explores such sensitivities whereas the LWC is constant but D_{wet} and N_a are varied. The simulations and experiments, as described in Sect. 2, have shown that oligomer formation in the laboratory experiments is highly sensitive to the dissolved oxygen concentrations. In highly concentrated ionic solutions (40 % salinity) as possibly encountered in highly-concentrated aerosol water, the solubility of oxygen is decreased by factor of ∼ 5 (Battino et al., 1983). In order to

ACPD
14, 21565–21609, 2014

mimic an atmospherically-relevant change in oxygen solubility, in Case C the Henry's law constant for oxygen is reduced by a factor of two to $K_{H,O_2(5)} = 0.0008\,M\,atm^{-1}$.

All model simulations so far assume that MVK is the only organic compound in the aqueous phase. However, the aqueous phase of aerosol particles usually contains hundreds of water-soluble organic compounds (WSOC), less of 50 % of which can be typically identified on a molecular level (Herckes et al., 2013). All of them could potentially react with OH in the aqueous phase (Reaction R1), resulting in alkyl radicals R(org)· that subsequently form peroxy radicals RO_2(org) (Reaction R2).

$$WSOC + OH \rightarrow R(org)\cdot \quad (R1)$$

$$R(org)\cdot + O_2 \rightarrow RO_2(org) \quad (R2)$$

These aqueous phase reactions were added to the mechanism to account for additional OH and O_2 losses. The further fate of the organic peroxy radicals RO_2(org) is not tracked. Based on the analysis in cloud and fog water samples, it has been recently suggested that the average rate constant for Reaction (R1) is $k_{WSOC} = 3.2\times10^8\,M^{-1}\,s^{-1}$ (Arakaki et al., 2013). The rate constant for Reaction (R2) is assumed to be identical to $k_{O_2} = 3.1\times10^9\,M^{-1}\,s^{-1}$ (Alfassi, 1997). We assume a total WSOC concentration of 0.1 M that does not change over the time scale of the simulation (Case D in Table 3). The total WSOC concentration in aerosol water might be much higher (1–10 M) (Lim et al., 2010); however, our conservative estimate takes into account the possibility that not all organics might be fully dissolved, and/or that they form separate phases and might not be available for aqueous phase reactions. In Case E, we assume that Reaction (R1) does not efficiently consume OH, i.e. Reaction (R1) does not act as an effective OH sink (i.e., the only OH sink is the reaction by MVK) and only forms R(org)· radicals; thus, in these simulations, the OH concentration is the same as in Case A. This assumption is justified by the facts that (i) this reaction likely leads to formation of HO_2 that, in turn, becomes recycled to OH (HO_x reactions in Table 1) and (ii) additional aqueous OH sources (e.g. Fenton reaction) might exist in aerosol particles that replenish the OH concentration instantaneously.

ACPD
14, 21565–21609, 2014

3.3 Model results

3.3.1 Surface-to-volume ratio

Figure 6a shows the predicted oligomer masses for the five cases as described above. As opposed to Fig. 4a, here the oligomer mass is expressed in units of ng m^{-3}, using a conversion factor assuming an average chain length of $n = 5$ for all oligomer series as found in the experiments (Sect. 2.1.2). Since this is only an approximate molecular weight, the exact oligomer masses might differ by several percent, if the true chain length is different, respectively. Figure 6a shows that – while the predicted oligomer formation continues to increase in Case A – it starts decreasing after ~ 100 min in Case B. Due to the higher surface-volume ratio, both MVK and OH are more readily transported in the aqueous phase. Since OH-initiated aqSOA formation is often predicted to be limited by OH (Ervens et al., 2014), its enhanced uptake rate, favored by a higher surface-to-volume ratio, lead to a higher OH concentration and, in turn, to somewhat smaller MVK concentration (Table 3). Since the MVK concentration is much higher than that of OH, the enhanced MVK uptake rate does not compensate for this loss. MVK is more quickly consumed and the resulting oligomers are more efficiently oxidized by OH, leading to the faster decrease in oligomer mass. The fact that these different oligomer formation rates are mostly due to the different OH concentrations (8×10^{-13} M vs. 2×10^{-12} M, Table 3) is also supported by the very similar oxygen concentrations for the two cases (Fig. 6b). Since usually the main OH source in the aqueous phase is the direct uptake from the gas phase, [OH(aq)] is not only dependent on its reactants (e.g. WSOC) but also on the time of the day (zenith angle). While we use a constant OH(gas) concentration and aqueous phase photolysis rate $j_{H_2O_2}$ for all simulations, changes in these parameters might affect OH-initiated oligomerization to a similar extent than other factors affecting OH(aq).

ACPD
14, 21565–21609, 2014

3.3.2 The role of O_2 solubility and consumption

If the amount of oxygen that can dissolve in the aqueous phase is lower by a factor of two as compared to Case A, the predicted oligomer mass is higher by ~ 40 % (Case C, Fig. 6a), in agreement with results in Fig. 2a vs. Fig. 2e. While it is not clear, whether oxygen solubility is indeed reduced in aerosol water, our sensitivity studies show that its concentration might significantly affect oligomerization rates. We caution here that these model studies are very exploratory, since the oligomerization rate does not depend on the absolute oxygen amount, but rather on the concentration ratio of MVK to oxygen. The MVK concentration in our model study is set by our somewhat arbitrary assumption of $K^*_{H,MVK}$, which could be quite different depending on the amount of aerosol water and composition.

If additional sinks for OH and O_2 are introduced (Reactions R1 and R2, respectively), the OH concentration in the aqueous phase is reduced by almost an order of magnitude as compared to Case A (OH(aq) = 10^{-13} M, Case D, Table 3). In that case, MVK is less efficiently oxidized to alkyl radicals that can form oligomers and the total oligomer mass is reduced by a factor of ~ 3 as compared to Case A (Fig. 6a). If Reaction (R1) does not act as an OH sink (Case E), the resulting OH concentration is identical to that in Case A. However, since Reaction (R2) efficiently consumes oxygen, its concentration decreases over the course of the simulation (Fig. 6b), and oligomerization is accelerated leading to slightly higher masses than in Case A (210 ng m^{-3} vs. 160 ng m^{-3}, respectively).

Overall the sensitivity studies above show that the oligomerization rate strongly depends on the microphysical characteristics of an aerosol population (D_{wet}, N_a), but also on the concentration and reactivity of the organics (WSOC and MVK) that control the oxygen concentration in the aqueous phase. Given the numerous uncertainties in the chemical mechanism, our model predictions might not be fully quantitative; however, the simulations clearly show that (i) aqSOA mass yields, related to the initial gas phase MVK concentration are in a range of ~ 1–10 % and that (ii) depending on assumptions

ACPD
14, 21565–21609, 2014

on solubility and surface–volume ratio, the oxygen uptake rates might impact these yields.

4 Atmospheric implications

4.1 AqSOA formation from isoprene

It can be expected that not only MVK, but also structurally similar compounds might initiate oligomerization via radical pathways; such compounds include unsaturated water-soluble organic compounds (UWSOC). One of these compounds is methacrolein (MACR) that represents the other main first-generation oxidation product from isoprene. MVK and MACR are formed with gas phase yields of 29 % and 21 % (with some variation, depending on NO_x levels), respectively (Galloway et al., 2011). Bulk aqueous phase experiments have shown that also methacrolein (MACR) efficiently forms oligomers in the aqueous phase (ElHaddad et al., 2009; Yao Liu et al., 2009; Michaud et al., 2009), but mechanistic information as detailed as for MVK is not available. MACR is less soluble than MVK ($K_{H,MACR} = 6.5\,M\,atm^{-1}$), but it has a slightly higher rate constant with OH in the aqueous phase, $k_{MACROH} = 9.4\times10^{9}\,M^{-1}\,s^{-1}$ (Schöne et al., 2014). The mass yields of oligomers from MACR are similar to those as observed for MVK; however, the diversity of detected oligomer series is higher (Liu et al., 2012). Instead of developing an explicit chemical mechanism for MACR, in the following, we only estimate its potential SOA formation efficiency scaled by that of MVK, given that both its OH reactivity and its overall oligomerization potential are known.

While the initial MACR decay might be somewhat faster than that for MVK, we assume that the kinetics of the subsequent MACR decay due to oligomerization and oligomer formation is comparable to that of MVK. Overall, the oligomer formation can then be approximated by a single reaction:

MVK or MACR + OH → Oligomers (R3)

ACPD
14, 21565–21609, 2014

In order to estimate the rate constant for Reaction (R3), $k_{R\text{-}3}$, we seek a rate constant that represents best the oligomer formation as predicted by the explicit mechanism in Fig. 1. In Fig. S3 in the Supplement, the solid lines are identical to those as for Cases A–E in Fig. 6. The other lines show model results for which the reactions involving MVK (i.e. initial OH reaction and the subsequent oligomerization steps) were replaced by Reaction (R3) with different $k_{R\text{-}3}$. While it is obvious that such a single reaction step cannot fully reproduce the wide range of oligomerization rates as predicted by the explicit mechanism, $k_{R\text{-}3}$ can be bounded by $1 \times 10^9\,M^{-1}\,s^{-1} < k_{R\text{-}3} < 1.5 \times 10^9\,M^{-1}\,s^{-1}$ as it reproduces for most cases both the temporal evolution and the final oligomer mass reasonably well. Only for Case C, i.e., for lower oxygen solubility, the oligomer formation rate is higher and $k_{R\text{-}3} = 2 \times 10^9\,M^{-1}\,s^{-1}$ seems more appropriate. In the following model studies, we use therefore an average value of $k_{R\text{-}3} = 1.5 \times 10^9\,M^{-1}\,s^{-1}$ in order to describe the OH-initiated oligomerization from MACR, whereas we apply the full mechanism (Fig. 1 and Table 1) for MVK. We do not suggest that oligomerization by any of these compounds should be indeed represented by R-3 in future model studies, since both the temporal evolution and the kinetics might be different for other conditions (N_a, LWC, [OH(aq)], [WSOC] etc). The only purpose of $k_{R\text{-}3}$ is to develop a shortcut that allows us to implement oligomerization from MACR in our model and to roughly estimate and compare its aqSOA formation potential.

4.2 Comparison to gasSOA formation

In the gas phase, only MACR forms SOA whereas MVK does not show any (detectable) SOA formation (Kroll et al., 2006; Surratt et al., 2006). SOA yields from isoprene are in the range of ~ 0–5 %, depending on oxidant, RH and NO_x levels (Carlton et al., 2009), and irradiation sources employed (Carter et al., 1995; Bregonzo-Rozier et al., 2014). In order to explore the simultaneous SOA formation from isoprene in the gas and aqueous phases, we simulate the multiphase system as shown in Fig. 7. The kinetic data for gas phase reactions and uptake processes are summarized in Table 4. For simplicity, the SOA yield from MACR is adjusted such that the overall gasSOA yield is

ACPD
14, 21565–21609, 2014

~ 2 % (= 21 % yield of MACR from isoprene multiplied by 10 % SOA yield from MACR, resulting in a value (2.1 %) that is in the range of observed SOA yields from isoprene). The other products (volatile organic compounds, VOCs) are not further tracked in the model, since they do not contribute to SOA mass. AqSOA formation from MVK occurs via the mechanism displayed in Fig. 1 and Table 1; aqSOA formation from MACR is approximated by $k_{R\text{-}3}$. The model is initialized with 2 ppb isoprene and 5×10^6 cm^{-3} OH in the gas phase, both of which are kept constant; initial values for MVK and MACR are set to zero.

Simulations are performed for model cases listed in Table 3 over 6 h. Results are shown in Fig. 8 after two and 6 h of simulation time, respectively. GasSOA masses are not affected by the choice of aerosol conditions (N_a, D_{wet}, LWC etc) and, thus, are identical for all simulations, since OH and MVK concentrations are not affected by different loss rates into the aqueous phase. The aqSOA formation rate is slower than that of gasSOA formation: at t = 2 h aqSOA is ~ 20 % of gasSOA mass (Cases A, B, and D) whereas its contribution increases to ~ 30 % after 6 h. Results for Case F (doubled LWC as compared to Case A) show that aqSOA formation is non-linear to total LWC due to the loss processes of OH and oxygen to the air–water interface and their subsequent consumption that do not scale with the total surface area.

It should be cautioned here that the results for cases A–F are all based on the assumption that both MVK and MACR partition into aerosol water 50 000 times more strongly than into pure water (i.e. $K_H \cdot 50\,000$, cf Sect. 3.1). To our knowledge, there is no direct measurement of the gas/particle partitioning available for MVK and MACR on ambient particles. If the K_H^* values were (arbitrarily chosen) smaller by two orders of magnitude, the amount of aqSOA from oligomerization is negligible and amounts to < 0.2 ng m^{-3} after 6 h (Case G in Table 3 and Fig. 8). However, one should keep in mind that MACR and MVK are only two selected precursors that lead to oligomers in the aqueous phase. Many additional structurally similar compounds (UWSOC) exist in the atmosphere that likely undergo similar chemical reactions. Their total concentration

ACPD
14, 21565–21609, 2014

in the aqueous phase of aerosol particles might be substantial and increase total aqSOA mass due to radical oligomerization.

Unlike in chamber experiments, we assume a constant mixing ratio of isoprene (2 ppb) throughout the simulation. Therefore, the total SOA mass cannot be directly related to this initial mixing ratio in order to calculate a SOA yield as done in laboratory experiments. The ratio of resulting SOA mass to initial isoprene is ~ 3 % for gasSOA after 6 h (180 ng m^{-3}/2 ppb) whereas it is in a range of < 0.01–3.4 % for aqSOA. The upper limit is for the highest LWC (Case F), which can only occur at high particle loading and hygroscopicity and/or high RH. In the latter case, it is likely that the particles are more dilute, and thus, K^*_H for MACR and MVK is likely smaller if the ionic strength of aerosol water is indeed a factor that determines the partitioning. Overall, our comparison to gasSOA production from isoprene suggest that oligomerization in the aqueous phase of aerosol water could be an additional source of SOA that should not be neglected under favorable (e.g., high RH) conditions. However, our sensitivity studies also reveal that the partitioning of MVK ($K^*_{H,MVK}$) is one of the main uncertainties in estimating the importance of this SOA formation pathway, together with the solubility and availability of oxygen in the aqueous phase.

Based on several bulk aqueous laboratory experiments (e.g. Part I, and Renard et al., 2013) aqSOA yields of nearly 100 % have been reported for oligomerization from MVK. The multiphase model simulations as performed here show that such values should be discussed with caution in the context of atmospheric implications. Only if simultaneous gas phase losses and uptake rates into the aqueous phase are taken into account, a fair comparison of aqSOA and gasSOA yields is feasible. Our simulations show that, even if 100 % of dissolved aqSOA precursors (MVK, MACR) is converted into oligomers, the overall aqSOA yield in the multiphase system might be significantly smaller (< 0.1–3.4 % as an upper limit; even smaller if isoprene were assumed to be consumed during the simulation), depending on aqSOA precursor solubility and microphysical characteristics of the aerosol size distribution.

ACPD
14, 21565–21609, 2014

5 Summary and conclusions

We have derived a chemical mechanism of the oligomerization of methyl vinyl ketone (MVK) in the aqueous phase, based on bulk aqueous phase laboratory studies that are described in previous work (Renard et al., 2013, 2014 (Part I)). Using this mechanism, model studies mimic the observed decay of MVK for a wide range of initial concentrations ($0.2\,\mathrm{mM} \leq [\mathrm{MVK(aq)}]_0 \leq 20\,\mathrm{mM}$). The different oligomerization rates for high and low aqueous phase concentrations of oxygen, respectively, can be reproduced by the model. This sensitivity occurs because alkyl radicals that are formed by OH oxidation of MVK can react either with oxygen forming peroxy radicals or with another MVK molecule, which leads to oligomers.

The chemical mechanism is implemented into a multiphase box model that is initialized with MVK (1 ppb) and OH in the gas phase. Under atmospherically relevant conditions, up to several hundred $\mathrm{ng\,m^{-3}}$ oligomer mass are predicted to form over the course of 6 h. The solubility of oxygen in aerosol water, together with oxygen's consumption rate by other organics in the aerosol aqueous phase, emerge as important parameters that determine the oligomerization rate in the atmospheric multiphase system. MVK, together with methacrolein (MACR) represent the main oxidation products of isoprene in the atmosphere. Even small SOA yields from isoprene oxidation products in the gas phase have been considered to contribute substantially to the total global SOA burden due to the high emission rate of isoprene. In an exploratory study, we compared the potential additional contributions of MVK and MACR oligomerization in the aerosol aqueous phase to the total SOA mass. Our model results show that at high relative humidity, aerosol loading and hygroscopicity, i.e., when the available aerosol liquid water content is substantial ($\sim 40\,\mathrm{\mu g\,m^{-3}}$), oligomerization in aerosol particles might contribute as much SOA as condensation of gas phase oxidation products to preexisting particles. However, this assumption implies that the partitioning of MVK and MACR into aqueous aerosol exceeds that predicted by their Henry's law constants by several orders of magnitude. While interactions of other highly concentrated

ACPD
14, 21565–21609, 2014

compounds in the bulk aqueous phase could favor such behavior, the accumulation of organic compounds at the air/water interface could lead to enhanced partitioning to the condensed phase. Such effects would enable heterogeneous reactions that might occur with similar mechanisms as discussed in the current study but with possibly higher rates due to the greater availability of aqSOA precursors in/on the condensed phase to gas phase oxidants. While simultaneous measurements of carbonyl concentrations in gas and particle phase do support such trends, these assumptions need to be corroborated further specifically for MVK and MACR.

The Supplement related to this article is available online at doi:10.5194/acpd-14-21565-2014-supplement.

Acknowledgements. All authors are thankful to V. Vaida and B. Ellison for valuable discussions on the chemical mechanism. B. Ervens acknowledges support from NOAA's climate goal. A. Monod acknowledges support from CIRES (visiting fellowship) and the National Research Agency ANR (project CUMULUS ANR-2010-BLAN-617-01), P. Renard acknowledges AXA insurances for funding this research.

References

Alfassi, Z. B.: The Chemistry of Free Radicals: Peroxyl Radicals, 1st Edn., Wiley, West Sussex, England, 1997.

Altieri, K. E., Turpin, B. J., and Seitzinger, S. P.: Oligomers, organosulfates, and nitrooxy organosulfates in rainwater identified by ultra-high resolution electrospray ionization FT-ICR mass spectrometry, Atmos. Chem. Phys., 9, 2533–2542, doi:10.5194/acp-9-2533-2009, 2009.

Arakaki, T., Anastasio, C., Kuroki, Y., Nakajima, H., Okada, K., Kotani, Y., Handa, D., Azechi, S., Kimura, T., Tsuhako, A., and Miyagi, Y.: A general scavenging rate constant for reaction of hydroxyl radical with organic carbon in atmospheric waters, Environ. Sci. Technol., 47, 8196–8203, doi:10.1021/es401927b, 2013.

ACPD
14, 21565–21609, 2014

Atkinson, R.: Kinetics and mechanisms of the gas-phase reactions of the hydroxyl radical with organic compounds under atmospheric conditions, Chem. Rev., 86, 69–201, doi:10.1021/cr00071a004, 1986.
Baboukas, E. D., Kanakidou, M., and Mihalopoulos, N.: Carboxylic acids in gas and particulate phase above the Atlantic Ocean, J. Geophys. Res., 105, 14459–14471, 2000.
Battino, R., Rettich, T. R., and Tominaga, T.: The solubility of oxygen and ozone in liquids, J. Phys. Chem. Ref. Data, 12, 163–178, 1983.
Bielski, B. H. J., Cabell, D. E., Arudi, R. L., and Ross, A. B.: Reactivity of HO_2/O_2^- radicals in aqueous solution, J. Phys. Chem. Ref. Data, 14, 1041–1100, 1985.
Blanksby, S. J. and Ellison, G. B.: Bond dissociation energies of organic molecules, Accounts Chem. Res., 36, 255–263, doi:10.1021/ar020230d, 2003.
Carlton, A. G., Wiedinmyer, C., and Kroll, J. H.: A review of Secondary Organic Aerosol (SOA) formation from isoprene, Atmos. Chem. Phys., 9, 4987–5005, doi:10.5194/acp-9-4987-2009, 2009.
Carter, W. P. L., Luo, D., Malkina, I. L., and Pierce, J. A.: Chamber studies of atmospheric reactivities of volatile organic compounds. Effects of varying chamber and light source, California Air Resources Board, South Coast Air Quality Management District Coordinating Research Council, Inc., 1995.
Chin, M. and Wine, P. H.: A temperature-dependent competitive kinetics study of the aqueous-phase reactions of OH radicals with formate, formic acid, acetate, acetic acid and hydrated formaldehyde, in: Aquatic and Surface Photochemistry, edited by: Helz, G. R., Zepp, R. G., and Crosby, D. G., Lewis Publishers, Boca Raton, 85–96, 1994.
Christensen, H., Sehested, K., and Corfitzen, H.: Reactions of hydroxyl radicals with hydrogen peroxide at ambient and elevated temperatures, J. Phys. Chem., 86, 1588–1590, doi:10.1021/j100206a023, 1982.
Denkenberger, K. A., Moffet, R. C., Holecek, J. C., Robetier, T. P., and Prather, K. A.: Real-time, single-particle measurements of oligomers in aged ambient aerosol particles, Environ. Sci. Technol., 41, 5439–5446, 2007.
Donahue, N. M., Robinson, A. L., Stanier, C. O., and Pandis, S. N.: Coupled partitioning, dilution and chemical aging of semivolatile organics, Environ. Sci. Technol., 40, 2635–2643, 2006.
Donahue, N. M., Epstein, S. A., Pandis, S. N., and Robinson, A. L.: A two-dimensional volatility basis set: 1. organic-aerosol mixing thermodynamics, Atmos. Chem. Phys., 11, 3303–3318, doi:10.5194/acp-11-3303-2011, 2011.

ACPD
14, 21565–21609, 2014

Donaldson, D. J. and Valsaraj, K. T.: Adsorption and reaction of trace gas-phase organic compounds on atmospheric water film surfaces: a critical review, Environ. Sci. Technol., 44, 865–873, doi:10.1021/es902720s, 2010.

Doussin, J.-F. and Monod, A.: Structure–activity relationship for the estimation of OH-oxidation rate constants of carbonyl compounds in the aqueous phase, Atmos. Chem. Phys., 13, 11625–11641, doi:10.5194/acp-13-11625-2013, 2013.

El Haddad, I., Yao Liu, Nieto-Gligorovski, L., Michaud, V., Temime-Roussel, B., Quivet, E., Marchand, N., Sellegri, K., and Monod, A.: In-cloud processes of methacrolein under simulated conditions – Part 2: Formation of secondary organic aerosol, Atmos. Chem. Phys., 9, 5107–5117, doi:10.5194/acp-9-5107-2009, 2009.

Elliot, A. J. and Buxton, G. V.: Temperature dependence of the reactions $OH + O_2^-$ and $OH + HO_2$ in water up to 200 °C, J. Chem. Soc. Faraday T., 88, 2465–2470, 1992.

Epstein, S. A., Tapavicza, E., Furche, F., and Nizkorodov, S. A.: Direct photolysis of carbonyl compounds dissolved in cloud and fog droplets, Atmos. Chem. Phys., 13, 9461–9477, doi:10.5194/acp-13-9461-2013, 2013.

Ervens, B., Gligorovski, S., and Herrmann, H.: Temperature dependent rate constants for hydroxyl radical reactions with organic compounds in aqueous solution, Phys. Chem. Chem. Phys., 5, 1811–1824, 2003.

Ervens, B., Turpin, B. J., and Weber, R. J.: Secondary organic aerosol formation in cloud droplets and aqueous particles (aqSOA): a review of laboratory, field and model studies, Atmos. Chem. Phys., 11, 11069–11102, doi:10.5194/acp-11-11069-2011, 2011.

Ervens, B., Sorooshian, A., Lim, Y. B., and Turpin, B. J.: Key parameters controlling OH-initiated formation of secondary organic aerosol in the aqueous phase (aqSOA), J. Geophys. Res., 119, 3997–4016, doi:10.1002/2013JD021021, 2014.

Galloway, M. M., Huisman, A. J., Yee, L. D., Chan, A. W. H., Loza, C. L., Seinfeld, J. H., and Keutsch, F. N.: Yields of oxidized volatile organic compounds during the OH radical initiated oxidation of isoprene, methyl vinyl ketone, and methacrolein under high-NO_x conditions, Atmos. Chem. Phys., 11, 10779–10790, doi:10.5194/acp-11-10779-2011, 2011.

Gilbert, B. C., Smith, J. R. L., Milne, E. C., Whitwood, A. C., and Taylor, P.: Kinetic and structural EPR studies of radical polymerization. Monomer, dimer, trimer and mid-chain radicals formed via the initiation of polymerization of acrylic acid and related compounds with electrophilic radicals ([radical dot]OH, SO_4-[radical dot] and Cl_2-[radical dot]), J. Chem. Soc. Perk. T. 2, 8, 1759–1769, doi:10.1039/p29940001759, 1994.

ACPD
14, 21565–21609, 2014

Guzman, M. I., Colussi, A. J., and Hoffmann, M. R.: Photoinduced oligomerization of aqueous pyruvic acid, J. Phys. Chem. A, 110, 3619–3626, 2006.
Healy, R. M., Wenger, J. C., Metzger, A., Duplissy, J., Kalberer, M., and Dommen, J.: Gas/particle partitioning of carbonyls in the photooxidation of isoprene and 1,3,5-trimethylbenzene, Atmos. Chem. Phys., 8, 3215–3230, doi:10.5194/acp-8-3215-2008, 2008.
Herckes, P., Valsaraj, K. T., and Collett Jr., J. L.: A review of observations of organic matter in fogs and clouds: origin, processing and fate, Atmos. Res., 132–133, 434–449, doi:10.1016/j.atmosres.2013.06.005, 2013.
Iraci, L. T., Baker, B. M., Tyndall, G. S., and Orlando, J. J.: Measurements of the Henry's law coefficients of 2-methyl-3-buten-2-ol, methacrolein, and methylvinyl ketone, J. Atmos. Chem., 33, 321–330, 1999.
Kalberer, M., Paulsen, D., Sax, M., Steinbacher, M., Dommen, J., Prevot, A. S. H., Fisseha, R., Weingartner, E., Frankevich, V., Zenobi, R., and Baltensperger, U.: Identification of polymers as major components of atmospheric organic aerosols, Science, 303, 1659–1662, 2004.
Kanakidou, M., Seinfeld, J. H., Pandis, S. N., Barnes, I., Dentener, F. J., Facchini, M. C., Van Dingenen, R., Ervens, B., Nenes, A., Nielsen, C. J., Swietlicki, E., Putaud, J. P., Balkanski, Y., Fuzzi, S., Horth, J., Moortgat, G. K., Winterhalter, R., Myhre, C. E. L., Tsigaridis, K., Vignati, E., Stephanou, E. G., and Wilson, J.: Organic aerosol and global climate modelling: a review, Atmos. Chem. Phys., 5, 1053–1123, doi:10.5194/acp-5-1053-2005, 2005.
Kawamura, K., Okuzawa, K., Aggarwal, S. G., Irie, H., Kanaya, Y., and Wang, Z.: Determination of gaseous and particulate carbonyls (glycolaldehyde, hydroxyacetone, glyoxal, methylglyoxal, nonanal and decanal) in the atmosphere at Mt. Tai, Atmos. Chem. Phys., 13, 5369–5380, doi:10.5194/acp-13-5369-2013, 2013.
Kroll, J. H., Ng, N. L., Murphy, S. M., Varutbangkul, V., Flagan, R. C., and Seinfeld, J. H.: Chamber studies of secondary organic aerosol growth by reactive uptake of simple carbonyl compounds, J. Geophys. Res., 110, D23207, doi:10.1029/2005JD006004, 2005.
Kroll, J. H., Ng, N. L., Murphy, S. M., Flagan, R. C., and Seinfeld, J. H.: Secondary organic aerosol formation from isoprene photooxidation, Environ. Sci. Technol., 40, 1869–1877, 2006.
Lim, Y. B., Tan, Y., Perri, M. J., Seitzinger, S. P., and Turpin, B. J.: Aqueous chemistry and its role in secondary organic aerosol (SOA) formation, Atmos. Chem. Phys., 10, 10521–10539, doi:10.5194/acp-10-10521-2010, 2010.

ACPD
14, 21565–21609, 2014

Lim, Y. B., Tan, Y., and Turpin, B. J.: Chemical insights, explicit chemistry, and yields of secondary organic aerosol from OH radical oxidation of methylglyoxal and glyoxal in the aqueous phase, Atmos. Chem. Phys., 13, 8651–8667, doi:10.5194/acp-13-8651-2013, 2013.

Liu, Y., Monod, A., Tritscher, T., Praplan, A. P., DeCarlo, P. F., Temime-Roussel, B., Quivet, E., Marchand, N., Dommen, J., and Baltensperger, U.: Aqueous phase processing of secondary organic aerosol from isoprene photooxidation, Atmos. Chem. Phys., 12, 5879–5895, doi:10.5194/acp-12-5879-2012, 2012.

Long, T. E., McGrath, J. E., and Richard, S.: Polymers, Synthesis, pp. 751-774, in: Encyclopedia of physical science and technology, Polymers, 3rd Edn., edited by: Meyers, R. A., Academic Press, New York, 2001.

Mackay, D. and Shiu, W. Y.: A critical review of Henry's law constants for chemicals of environmental interest, J. Phys. Chem. Ref. Data, 10, 1175–1199, 1981.

Matsunaga, S. N., Kato, S., Yoshino, A., Greenberg, J. P., Kajii, Y., and Guenther, A. B.: Gas-aerosol partitioning of semi volatile carbonyls in polluted atmosphere in Hachioji, Tokyo, Geophys. Res. Lett., 32, L11805, doi:10.1029/2004gl021893, 2005.

Mazzoleni, L. R., Ehrmann, B. M., Shen, X., Marshall, A. G., and Collett, J. L.: Water-soluble atmospheric organic matter in fog: exact masses and chemical formula identification by ultrahigh-resolution Fourier transform ion cyclotron resonance mass spectrometry, Environ. Sci. Technol., 44, 3690–3697, doi:10.1021/es903409k, 2010.

Mead, R. N., Mullaugh, K. M., Brooks Avery, G., Kieber, R. J., Willey, J. D., and Podgorski, D. C.: Insights into dissolved organic matter complexity in rainwater from continental and coastal storms by ultrahigh resolution Fourier transform ion cyclotron resonance mass spectrometry, Atmos. Chem. Phys., 13, 4829–4838, doi:10.5194/acp-13-4829-2013, 2013.

Mendez, M., Ciuraru, R., Gosselin, S., Batut, S., Visez, N., and Petitprez, D.: Reactivity of chlorine radical with submicron palmitic acid particles: kinetic measurements and product identification, Atmos. Chem. Phys., 13, 11661–11673, doi:10.5194/acp-13-11661-2013, 2013.

Michaud, V., El Haddad, I., Yao Liu, Sellegri, K., Laj, P., Villani, P., Picard, D., Marchand, N., and Monod, A.: In-cloud processes of methacrolein under simulated conditions – Part 3: Hygroscopic and volatility properties of the formed secondary organic aerosol, Atmos. Chem. Phys., 9, 5119–5130, doi:10.5194/acp-9-5119-2009, 2009.

Monod, A., Chebbi, A., Durand-Jolibois, R., and Carlier, P.: Oxidation of methanol by hydroxyl radicals in aqueous solution under simulated cloud droplet conditions, Atmos. Environ., 34, 5283–5294, 2000.

ACPD
14, 21565–21609, 2014

Monod, A., Poulain, L., Grubert, S., Voisin, D., and Wortham, H.: Kinetics of OH-initiated oxidation of oxygenated organic compounds in the aqueous phase: new rate constants, structure–activity relationships and atmospheric implications, Atmos. Environ., 39, 7667–7688, 2005.

Monod, A., Chevallier, E., Jolibos, R. D., Doussin, J. F., Picquet-Varrault, B., and Carlier, P.: Photooxidation of methylhydroperoxide and ethylhydroperoxide in the aqueous phase under simulated cloud droplet conditions, Atmos. Environ., 41, 2412–2426, 2007.

NDRL/NIST: Solution Kinetics Database on the Web, available at: http://kinetics.nist.gov/solution/ (last access: 29 July 2014), 2002.

Neta, P., Huie, R. E., and Ross, A. B.: Rate constants for reactions of peroxyl radicals in fluid solutions, J. Phys. Chem. Ref. Data, 19, 413–513, 1990.

Noziere, B., Voisin, D., Longfellow, C. A., Friedli, H., Henry, B. E., and Hanson, D. R.: The uptake of methyl vinyl ketone, methacrolein, and 2-methyl-3-butene-2-ol onto sulfuric acid solutions, J. Phys. Chem. A, 110, 2387–2395, 2006.

Odian, G.: Principles of Polymerization, John Wiley & Sons Inc., Hoboken, New Jersey, 835 pp., 2004.

Odum, J. R., Hoffmann, T., Bowman, F., Collins, D., Flagan, R. C., and Seinfeld, J. H.: Gas/particle partitioning and secondary organic aerosol yields, Environ. Sci. Technol., 30, 2580–2585, 1996.

Polidori, A., Turpin, B. J., Davidson, C. I., Rodenburg, L. A., and Maimone, F.: Organic $PM_{2.5}$: fractionation by polarity, FTIR Spectroscopy, and OM/OC ratio for the Pittsburgh aerosol, Aerosol Sci. Tech., 42, 233–246, 2008.

Reed-Harris, A., Ervens, B., Shoemaker, R. K., Griffith, E. C., Rapf, R. J., Kroll, J., Monod, A., and Vaida, V.: Photochemical kinetics of pyruvic acid in aqueous solution, J. Phys. Chem. A, doi:10.1021/jp502186q, 2014.

Renard, P., Siekmann, F., Gandolfo, A., Socorro, J., Salque, G., Ravier, S., Quivet, E., Clément, J.-L., Traikia, M., Delort, A.-M., Voisin, D., Vuitton, V., Thissen, R., and Monod, A.: Radical mechanisms of methyl vinyl ketone oligomerization through aqueous phase OH-oxidation: on the paradoxical role of dissolved molecular oxygen, Atmos. Chem. Phys., 13, 6473–6491, doi:10.5194/acp-13-6473-2013, 2013.

Renard, P., Siekmann, F., Salque, G., Smaani, A., Demelas, C., Coulomb, B., Vassalo, L., Ravier, S., Temime-Roussel, B., Voisin, D., and Monod, A.: Aqueous phase oligomerization of methyl vinyl ketone through photooxidation – Part 1: Aging processes of oligomers, Atmos. Chem. Phys. Discuss., 14, 15283–15322, doi:10.5194/acpd-14-15283-2014, 2014.

ACPD
14, 21565–21609, 2014

Schaefer, T., Schindelka, J., Hoffmann, D., and Herrmann, H.: Laboratory kinetic and mechanistic studies on the OH-initiated oxidation of acetone in aqueous solution, J. Phys. Chem. A, 116, 6317–6326, doi:10.1021/jp2120753, 2012.

Schöne, L., Schindelka, J., Szeremeta, E., Schaefer, T., Hoffmann, D., Rudzinski, K. J., Szmigielski, R., and Herrmann, H.: Atmospheric aqueous phase radical chemistry of the isoprene oxidation products methacrolein, methyl vinyl ketone, methacrylic acid and acrylic acid – kinetics and product studies, Phys. Chem. Chem. Phys., 16, 6257–6272, doi:10.1039/c3cp54859g, 2014.

Schwartz, S.: Mass transport considerations pertinent to aqueous phase reactions of gases in liquid water clouds, in: Chemistry of Multiphase Atmospheric Systems, edited by: Jaeschke, W., NATO ASI Series, Springer, Berlin, 415–471, 1986.

Surratt, J. D., Murphy, S. M., Kroll, J. H., Ng, N. L., Hildebrandt, L., Sorooshian, A., Szmigielski, R., Vermeylen, R., Maenhaut, W., Claeys, M., Flagan, R. C., and Seinfeld, J. H.: Chemical composition of secondary organic aerosol formed from the photooxdiation of isoprene, J. Phys. Chem. A, 110, 31,9665–9690, 2006.

Tolocka, M. P., Jang, M., Ginter, J. M., Cox, F. J., Kamens, R. M., and Johnston, M. J.: Formation of oligomers in secondary organic aerosol, Environ. Sci. Technol., 38, 1428–1434, 2004.

Trump, E. R. and Donahue, N. M: Oligomer formation within secondary organic aerosols: equilibrium and dynamic considerations, Atmos. Chem. Phys., 14, 3691–3701, doi:10.5194/acp-14-3691-2014, 2014.

Volkamer, R., Ziemann, P. J., and Molina, M. J.: Secondary Organic Aerosol Formation from Acetylene (C_2H_2): seed effect on SOA yields due to organic photochemistry in the aerosol aqueous phase, Atmos. Chem. Phys., 9, 1907–1928, doi:10.5194/acp-9-1907-2009, 2009.

Yao Liu, El Haddad, I., Scarfogliero, M., Nieto-Gligorovski, L., Temime-Roussel, B., Quivet, E., Marchand, N., Picquet-Varrault, B., and Monod, A.: In-cloud processes of methacrolein under simulated conditions – Part 1: Aqueous phase photooxidation, Atmos. Chem. Phys., 9, 5093–5105, doi:10.5194/acp-9-5093-2009, 2009.

Yu, G., Bayer, A. R., Galloway, M. M., Korshavn, K. J., Fry, C. G., and Keutsch, F. N.: Glyoxal in aqueous ammonium sulfate solutions: products, kinetics and hydration effects, Environ. Sci. Technol., 45, 6336–6342, doi:10.1021/es200989n, 2011.

Zhang, H. and Ying, Q.: Secondary organic aerosol formation and source apportionment in Southeast Texas, Atmos. Environ., 45, 3217–3227, doi:10.1016/j.atmosenv.2011.03.046, 2011.

ACPD
14, 21565–21609, 2014

Zhang, Q., Jimenez, J. L., Canagaratna, M. R., Allan, J. D., Coe, H., Ulbrich, I., Alfarra, M. R., Takami, A., Middlebrook, A. M., Sun, Y. L., Dzepina, K., Dunlea, E., Docherty, K., DeCarlo, P. F., Salcedo, D., Onasch, T., Jayne, J. T., Miyoshi, T., Shimono, A., Hatekayama, S., Takegawa, N., Kondo, Y., Schneider, J., Drewnick, F., Borrmann, S., Weiner, S., Demerijan, K., Williams, P., Bower, K., Bahreini, R., Cottrell, L., Griffin, R. J., Rautiainen, J., Sun, J. Y., Zhang, Y. M., and Worsnop, D. R.: Ubiquity and dominance of oxygenated species in organic aerosols in anthropogenically-influenced Northern Hemisphere midlatitudes, Geophys. Res. Lett., 34, L13801, doi:10.1029/2007GL029979, 2007.

Zhang, X., Chen, Z. M., and Zhao, Y.: Laboratory simulation for the aqueous OH-oxidation of methyl vinyl ketone and methacrolein: significance to the in-cloud SOA production, Atmos. Chem. Phys., 10, 9551–9561, doi:10.5194/acp-10-9551-2010, 2010.

ACPD
14, 21565–21609, 2014

Table 1. Rate constants (at 298 K) for the processes in Fig. 1.

Symbol	Description	k	Reference/Comment
$j_{H_2O_2}$	Photolysis of hydrogen peroxide	1.01×10^{-5} s^{-1}	Maximum value, cf discussion in Sect. 2.2.2 and Fig. 3 for adjustments as a function of $[MVK]_0$
$k_{MVKOH(a)}$	Oxidation of MVK by OH radical, H-abstraction from allyl group	7.18×10^9 M^{-1} s^{-1}	The total rate constant is $k_{MVKOH} = 7.3 \times 10^9$ M^{-1} s^{-1} Schöne et al. (2014) The branching ratio (98.4 %/1.6 %) was determined based on H-NMR studies
$k_{MVKOH(b)}$	Oxidation of MVK by OH radical, H-abstraction from methyl group	1.17×10^8 M^{-1} s^{-1}	
k_{O_2}	Peroxy radical formation from alkyl radicals	3.1×10^9 M^{-1} s^{-1}	Average value of rate constant $R\cdot + O_2$ Neta et al. (1990)
k_{olig}	Addition of nth MVK ($1 \le n \le 10$)	5×10^7 M^{-1} s^{-1}	$k = 10^2$–10^4 M^{-1} s^{-1} in Odian (2004)
k_{loss}	Oxidation of oligomers by OH radical	10^8 M^{-1} s^{-1}	Average k_{OH} for large organic compounds, e.g., Arakaki et al. (2013)
j_{ROOH}	Photolysis of hydroxyperoxides	Same as $j_{H_2O_2}$	
k_{1st}	Simplified 1st order reaction: conversion of oligomer radicals to stable products	6×10^4 s^{-1}	Estimated in order to reproduce observed increase in oligomer mass (Sect. 2.2.4)
k_{arr}	Rearrangement reaction	8×10^6 s^{-1}	
k_{recomb}	Recombination of radicals	2.4×10^6 s^{-1}	Estimated as 30 % of k_{arr}
k_{MglyOH}	Oxidation of methylglyoxal by OH radical	6.1×10^8 M^{-1} s^{-1}	Schaefer et al. (2012)
k_{HAcOH}	Oxidation of acetic acid/acetate by OH radical	1.5×10^7 M^{-1} s^{-1} (HAc) 10^8 M^{-1} s^{-1} (Ac^-)	Chin (1994)
k_{HO_2}	Recombination reaction of RO_2 with HO_2/O_2^-	8×10^5M^{-1} s^{-1} (HO_2) 9.7×10^7 M^{-1} s^{-1} (O_2^-)	Estimated equal to HO_2 + HO_2/O_2^-

ACPD
14, 21565–21609, 2014

Table 1. Continued.

HO_x reactions		
$H_2O_2 + h\nu \rightarrow 2OH$	$j_{H_2O_2} = f([MVK]_0)$	Experimentally derived, cf. Fig. 3
$H_2O_2 + OH \rightarrow HO_2 + H_2O$	$3 \times 10^7\ M^{-1}\ s^{-1}$	Christensen et al. (1982)
$HO_2 + HO_2/O_2^- \rightarrow O_2 + H_2O_2$	$8 \times 10^5 M^{-1}\ s^{-1}$ (HO_2)	Bielski et al. (1985)
	$9.7 \times 10^7\ M^{-1}\ s^{-1}$ (O_2^-)	
$OH + HO_2/O_2^- \rightarrow H_2O + O_2$	$10^{10}\ M^{-1}\ s^{-1}$	Elliot and Buxton (1992)
WSOC reactions (Sect. 3.2)		
$WSOC + OH \rightarrow R\cdot + HO_2$	$3.8 \times 10^8\ M^{-1}\ s^{-1}$	Arakaki et al. (2013)
$R\cdot + O_2 \rightarrow RO_2$	$3.1 \times 10^9\ M^{-1}\ s^{-1}$	Neta et al. (1990)

ACPD
14, 21565–21609, 2014

Table 2. Initial conditions for box model multiphase simulations.

Parameter	Value
$K_{H\ MVK}^{a}$	2.1×10^{6} M atm^{-1}
Mass accommodation coefficient for all species	αg 1
Gas phase diffusion coefficient	$D_g = 2 \times 10^{-5}$ cm^2 s^{-1}
Diameter	$D_{wet} = 200$ nm
Concentration	$N_a = 5000$ cm^{-3}
LWC	20 µg m^{-3}
Gas phase mixing ratios or concentrations	
MVK[b]	1 ppb
Isoprene[b]	2 ppb
H_2O_2	1 ppb
O_2	0.21 atm
OH	5×10^{6} cm^{-3}

[a] The value applied for K_H here is estimated such that 0.1 % of MVK is present in the particulate phase. It exceeds the physical Henry's law constant by a factor 50 000 (cf. Sect. 3.1).
[b] Either of these concentrations is used. $[MVK]_0 = 0$ for the simulations in Sect. 4.

ACPD
14, 21565–21609, 2014

Table 3. Conditions for sensitivity studies using the multiphase box model (Figs. 6 and 8). The listed MVK(aq) and OH(aq) concentrations are the average concentrations within the first seconds of the model simulations. For Cases A–F, it is assumed that MVK (and MACR, only in Case F) partitions into the aqueous phase according to equilibrium constants that are 50 000 higher than the Henry's law constants.

Case #	D_{wet} nm	N cm^{-3}	LWC $\mu g\,m^{-3}$	K_H (O_2) $M\,atm^{-1}$	[WSOC] M	k_{WSOCOH} $M^{-1}\,s^{-1}$	[MVK(aq)] mM	[OH(aq)] M	Comment
A	200	5000	20	0.0013	0	0	2	8×10^{-13}	
B	100	40 000	20	0.0013	0	0	1.7	2×10^{-12}	
C	200	5000	20	0.0008	0	0	2	8×10^{-13}	
D	200	5000	20	0.0013	0.1	3.2×10^{8}	2	1×10^{-13}	Case A, including Reactions (R1) and (R2)
E	200	5000	20	0.0013	0.1	3.2×10^{8}	2	8×10^{-13}	Same as Case D but Reaction (R1) is not an OH sink
F*	200	10 000	40	0.0013	0	0	2	8×10^{-13}	
G*	200	5000	20	0.0013	0	0	2	8×10^{-13}	Same as A but $K_H^* = 500 \times K_{H,}^* = 2.1 \times 10^4\,M\,atm^{-1}$

* These cases are only discussed in Sect. 4, i.e., they are initialized with isoprene instead of MVK only.

ACPD
14, 21565–21609, 2014

Table 4. Kinetic parameters for gas phase reactions and Henry's law constants for the multiphase simulations to compare aqSOA and gasSOA formation from isoprene (Fig. 8).

	k ($cm^3\ s^{-1}$)	Reference
Gas phase reactions		
Isoprene + OH → 0.29MVK + 0.21MACR	1×10^{-10}	Atkinson (1986)
MVK + OH → VOC	1.85×10^{-11}	Atkinson (1986)
MACR + OH → VOC + 0.1SOA	3.07×10^{-11}	Atkinson (1986)
Henry's law constants		
	K_H ($M\ atm^{-1}$)	
MVK(gas) ⇔ MVK(aq)	41*	Iraci et al. (1999)
MACR(gas) ⇔ MACR(aq)	6.5*	Iraci et al. (1999)

* Note that these constants are assumed to be higher by factors of 50 000 or 500 for the multiphase simulations discussed in Sects. 3 and 4, in order to account for the observed higher partitioning of carbonyl compounds into aerosol water as compared to pure water (K_H).

ACPD
14, 21565–21609, 2014

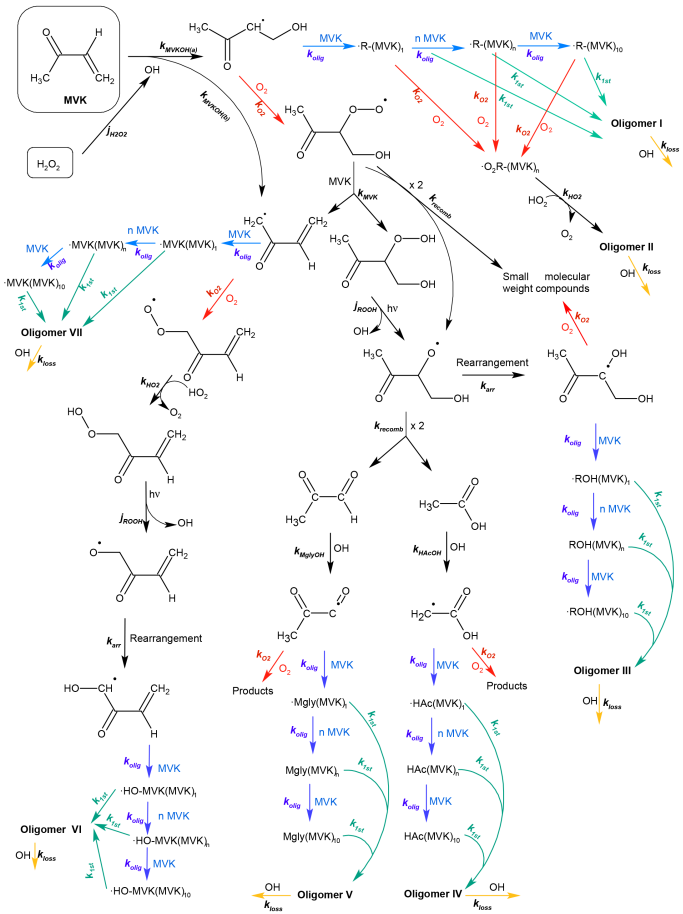

Figure 1. Chemical mechanism, constrained by laboratory studies for different conditions of $[MVK]_0$, $[H_2O_2]_0$. All rate constants are summarized in Table 1.

ACPD
14, 21565–21609, 2014

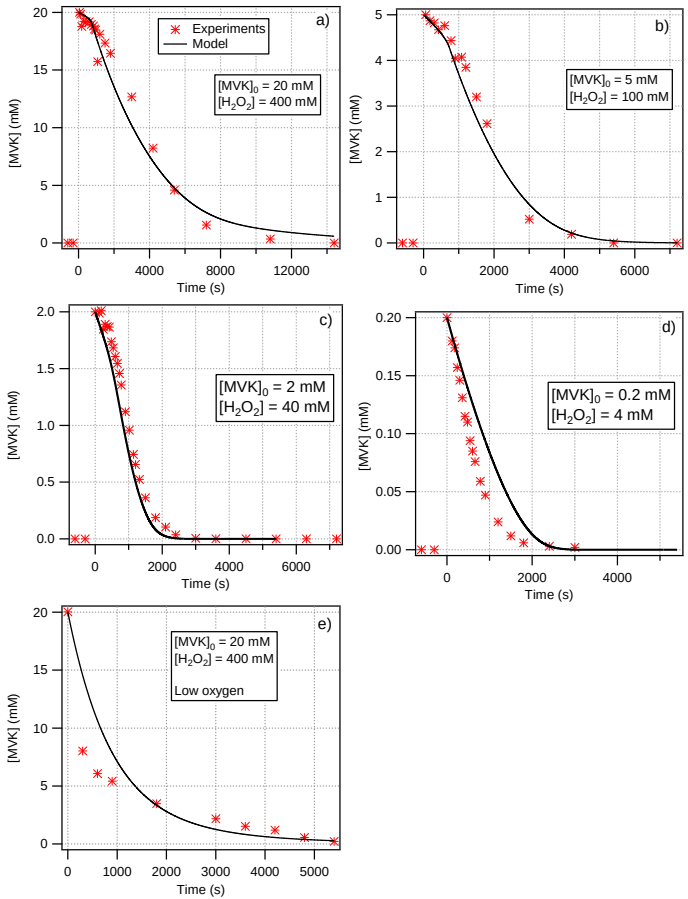

Figure 2. Comparison of experimental and model results using the mechanism listed in Table 1 and $j_{H_2O_2}$ in Fig. 3 for four initial MVK concentrations **(a)** 20 mM; **(b)** 5 mM; **(c)** 2 mM; **(d)** 0.2 mM. **(e)** $[MVK]_0$ = 20 mM; low oxygen concentration.

ACPD
14, 21565–21609, 2014

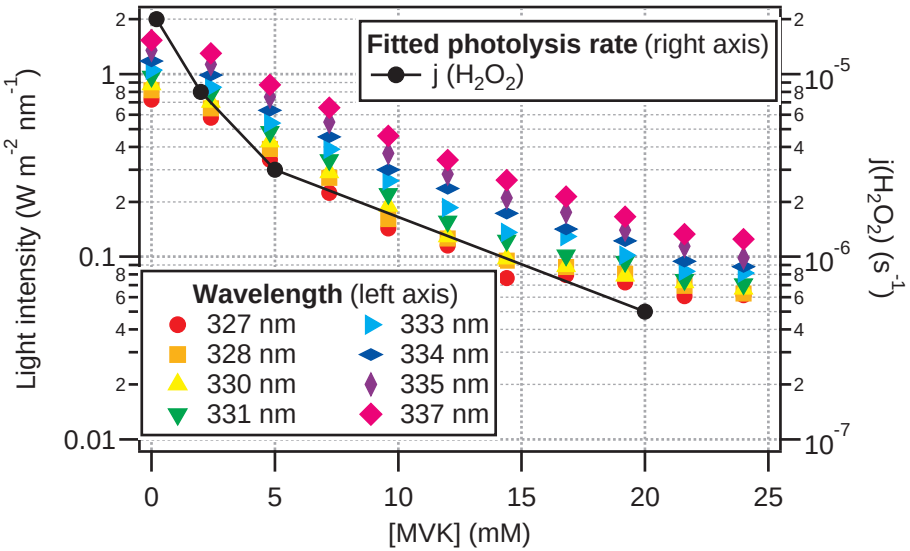

Figure 3. Light intensity of the lamp measured below the reactor at 3 different wavelengths, by means of a spectrophotometer, as function of MVK concentration (left axis) and photolysis rate constants, fitted in order to match MVK decay profiles for experiments with different initial MVK concentration (right axis).

ACPD
14, 21565–21609, 2014

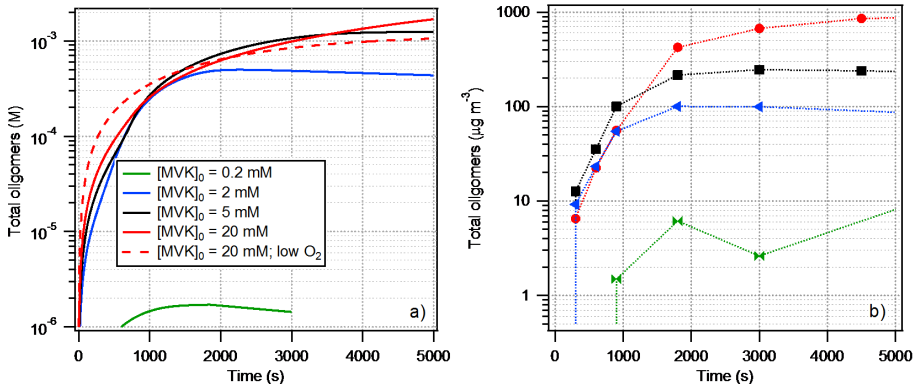

Figure 4. (a) Predicted oligomer concentrations (sum of all 6 oligomer series in Fig. 1) for different initial MVK concentrations (constant $[MVK]_0/[H_2O_2]_0$). **(b)** Total oligomer mass, determined by SMPS measurements from the nebulized solutions (see Fig. 7 by Renard et al., 2014, Part I).

ACPD
14, 21565–21609, 2014

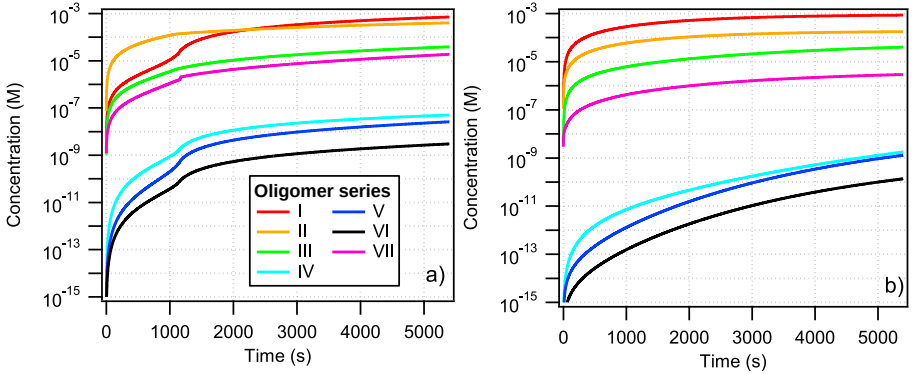

Figure 5. Comparison of predicted evolution for individual oligomer series I–VII (Fig. 1) for $[MVK]_0$ = 20 mM for **(a)** high (saturated) and **(b)** low initial oxygen concentrations.

ACPD
14, 21565–21609, 2014

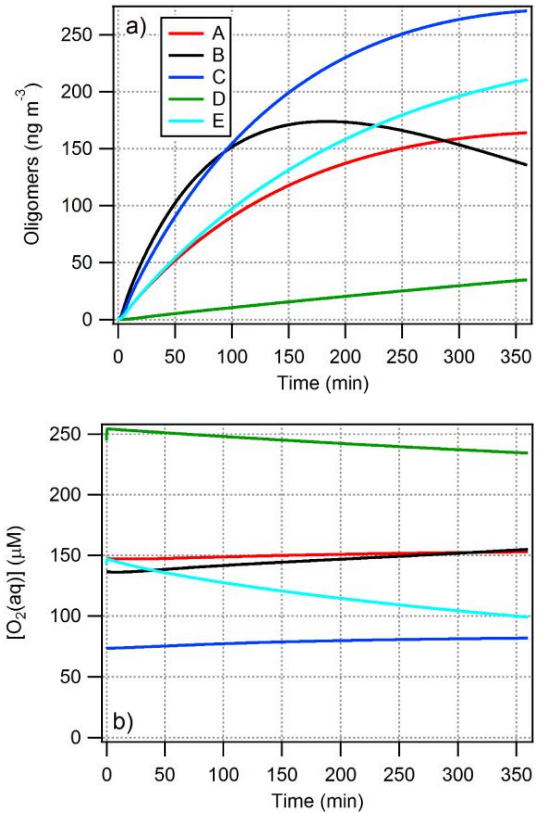

Figure 6. Results from the multiphase model for the cases listed in Table 3, **(a)** oligomer masses **(b)** oxygen concentrations in the aqueous phase.

ACPD
14, 21565–21609, 2014

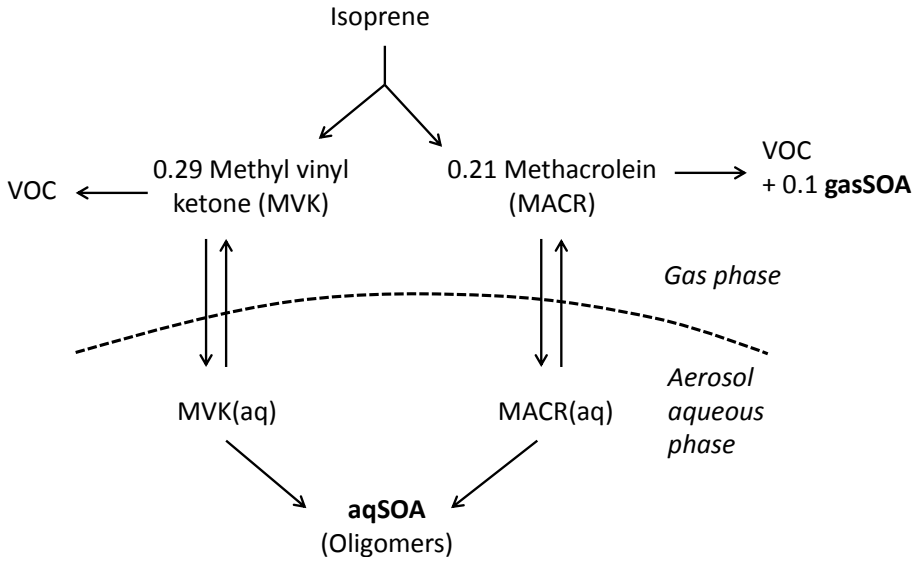

Figure 7. Schematic of SOA formation from isoprene in the atmospheric multiphase system; parameters for all processes are summarized in Tables 1 and 4.

ACPD
14, 21565–21609, 2014

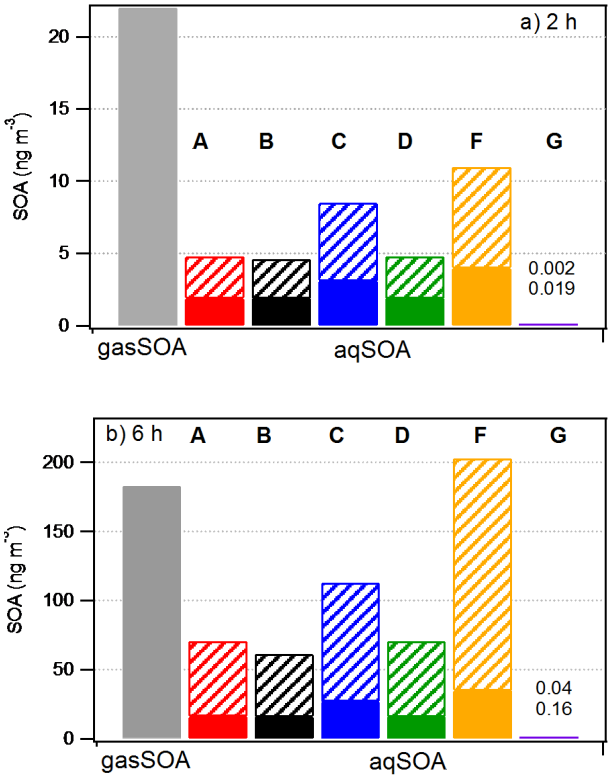

Figure 8. Comparison of aqSOA and gasSOA formation from isoprene for model cases for aqSOA in Table 3, solid bars for aqSOA denote predicted aqSOA mass from MACR, shaded bars denote predicted aqSOA mass from MVK.

ACPD
14, 21565–21609, 2014